Journal of Hazardous Materials 392 (2020) 122294

Contents lists available at ScienceDirect

Journal of Hazardous Materials

journal homepage: www.elsevier.com/locate/jhazmat

One minute synthesis of green fluorescent copper nanocluster: The preparation of smartphone aided paper-based kit for on-site monitoring of nanomolar level mercury and sulfide ions in environmental samples

Muniyandi Maruthupandi[a], Dharmaraj Thiruppathi[b], Nagamalai Vasimalai[a,*]

[a] Department of Chemistry, B.S. Abdur Rahman Crescent Institute of Science and Technology, Vandalur, Chennai, 600 048, India
[b] Department of Chemistry, Vivekananda College, Tiruvedakam West, Madurai, 625 234, India

GRAPHICAL ABSTRACT

Smartphone aided paper-based kit for Hg2+ and S2- sensor in environmental samples.

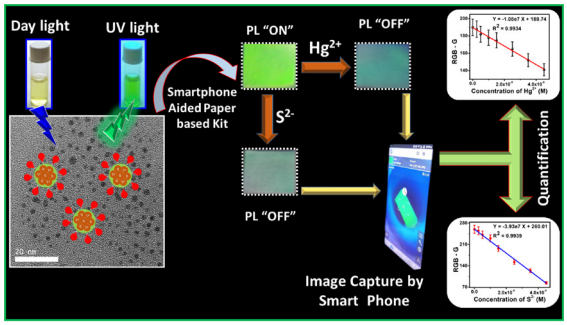

Smartphone aided paper-based kit for Hg^{2+} and S^{2-} sensor in environmental samples.

ARTICLE INFO

Editor: Danmeng Shuai

Keywords:
Copper nanocluster
Mercury
Sulfide
Spectrofluorimetry
Smartphone aided kit

ABSTRACT

We wish to report, a minute synthesis of green fluorescent copper nanocluster by simple sonication. 1-Thio-β-D-glucose was used as a capping ligand to synthesis copper nanocluster (TG-CuNCs). The TG-CuNCs exhibit the emission maximum at 430 nm. The synthesized TG-CuNCs was well characterized by UV–vis, fluorescent, XRD, HR-TEM and FT-IR techniques. After the addition of Hg^{2+} or S^{2-} into TG-CuNCs, the fluorescence was quenched. Based on the quenching of fluorescence, we have calculated the detection limit 1.7 nM and 1.02 nM for Hg^{2+} and S^{2-}, respectively. Finally, we have applied TG-CuNCs for the detection of Hg^{2+} and S^{2-} in tap, river, pond water. Importantly, the smartphone aided paper-based kit was developed for on-site monitoring of Hg^{2+} and S^{2-} ions. To the best of our knowledge, this is the first report for the one-minute synthesis of TG-CuNCs and the preparation of smartphone aided paper-based kit for on-site monitoring of Hg^{2+} and S^{2-} ions. Further, it is anticipated that this synthesis of TG-CuNCs and smartphone aided paper-based kit for Hg^{2+} and S^{2-} will be useful materials in the filled with the biosensor, material science and nanotechnology.

1. Introduction

Our environmental water is being polluted by several toxins due to the rapid industrialization. Importantly, toxic anions and cations can cause several health problems (Vaaramaa and Lehto, 2003). These anions and cations can exist into the water through various sources

* Corresponding author.
E-mail address: vasimalai@crescent.education (N. Vasimalai).

https://doi.org/10.1016/j.jhazmat.2020.122294
Received 18 November 2019; Received in revised form 11 February 2020; Accepted 12 February 2020
Available online 20 February 2020

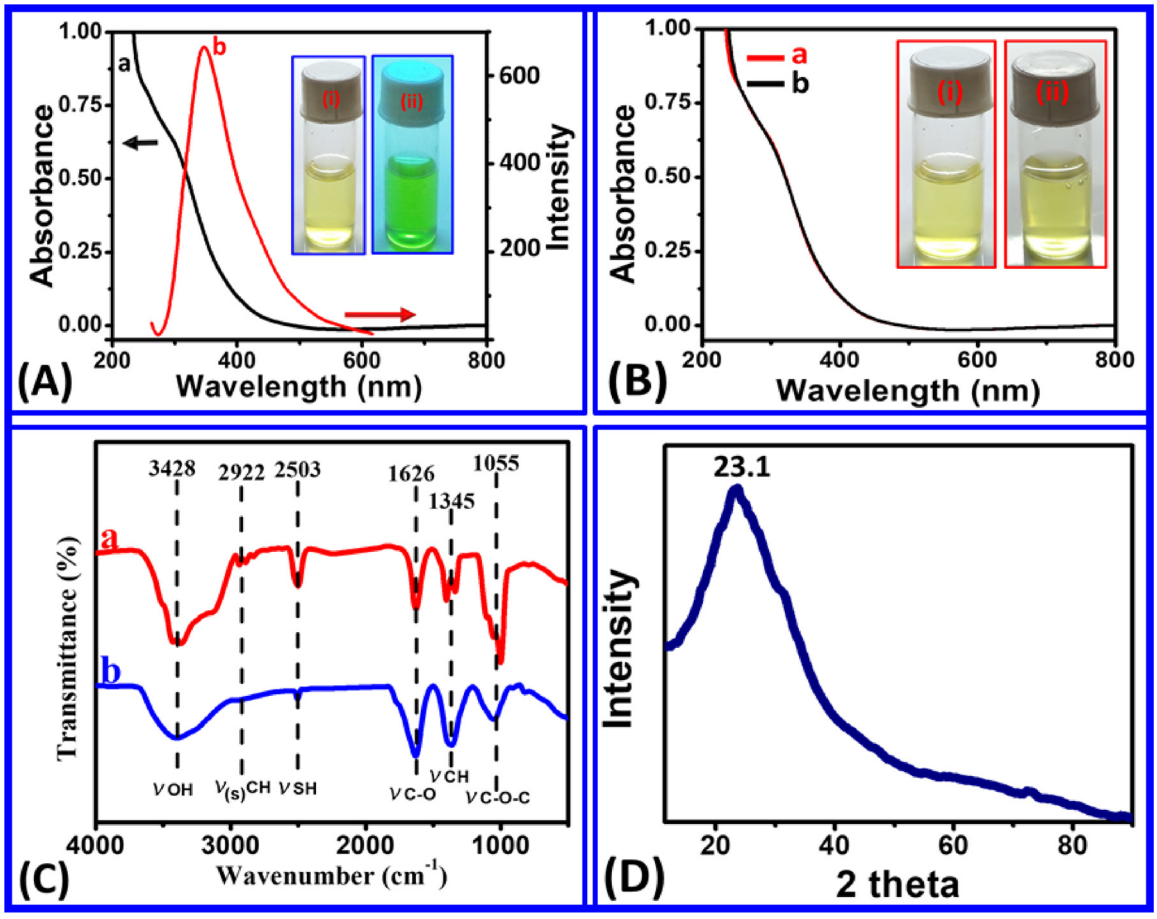

Fig. 1. (A) (a) UV–vis and (b) fluorescence spectrum of TG-CuNCs (λex:350, λem:430). Inset: Photograph of TG-CuNCs under (i) daylight and (ii) UV light (365 nm). (B) UV–vis spectra of (a) freshly prepared and (b) 2-months aged CuNCs. Inset: Corresponding photographs of freshly prepared (i) and 2-months aged TG-CuNCs (ii). (C) FT-IR spectra of (a) TG and (b) TG-CuNCs. (D) XRD pattern of TG-CuNCs.

including mining, volcanic emission, anthropogenic and natural sources (Jung, 2001; Bowen, 1979; Craig Cooper and Morse, 1998). For example, mercury toxicity is a serious concern. Mercury can exist through gold mining, volcanic emission and industrial sources. Mercury is extensively used for dental amalgam, electrical and electrolytic applications (WHO, 1996; Vasimalai and Abraham John, 2015; Huang and Chang, 2006). According to the United States Environmental Protection Agency 7500 tonnes mercury per year was released as waste into the environment. Mercury can damage kidney, heart, stomach and intestines (Craig Cooper and Morse, 1998; WHO, 1996; Vasimalai and Abraham John, 2015; Huang and Chang, 2006). Therefore, the World Health Organization has been recommended the level of Hg^{2+} is 5 μg/L, respectively (WHO, 1996; Vasimalai and Abraham John, 2015).

On the other hand, anion toxicity also considerable attention. In particularly, sulfide toxicity is a major concern. Sulfide ions play a role in the biological system. Sulfide can regulate the cardiovascular system activity, blood pressure, immune and apoptosis (Kang et al., 2019; Liang et al., 2015; Yuan et al., 2013; Vasimalai et al., 2018). Nonetheless, sulfide is major responsible anion for environmental pollution (Kang et al., 2019; Liang et al., 2015). Excess of sulfide can cause down syndrome and Alzheimer's disease and damage the cirrhosis and liver (Yuan et al., 2013; Vasimalai et al., 2018). Hence, the detection of Hg^{2+} and S^{2-} is essential today. Recent days, there are many methods available in the literature to detect Hg^{2+} and S^{2-} ions, such as atomic absorption spectrometry (Erxleben and Ruzicka, 2005; Afkhami and Khalafi, 2005), high performance liquid chromatography (Rekhi et al., 2017; Tang and Santschi, 2000), spectrofluorometer (Prodi et al., 2000; Guenther et al., 2001) and cyclic voltammetry technique etc., (Kanchana et al., 2015; Dilgin et al., 2012). Among the different techniques fluorescence method as vivid much alternation (Vasimalai et al., 2018; Cao et al., 2019; Huang et al., 2016; Lin et al., 2016; Liu et al., 2019a; Lin et al., 2017a, 2018). The synthesis of highly stable fluorescent copper nanocluster is a challenging task today. Copper nanocluster is extensively used in several fields including biosensor, catalysis, LED, bioimaging and water treatment etc., (Lu and Chen, 2012; Lin et al., 2017b; Aparna et al., 2019; Cao et al., 2014), due to their fascinating properties including smaller size, high surface area and low toxicity (Lu and Chen, 2012; Lin et al., 2017b; Aparna et al., 2019; Cao et al., 2014). Hence, it is needed to develop a new protocol for the synthesis of highly fluorescent copper nanocluster with a very short time (Gedanken, 2004; Ziarati et al., 2013).

Moreover, low-cost, smartphone aided portable kit preparation is essential today in the developing world and remote area for on-site monitoring of Hg^{2+} and S^{2-} ions.

Keeping these intentions in our mind, we have developed a new synthesis protocol for the preparation of CuNCs. Herein, we are reporting a highly fluorescent copper nanocluster, which was synthesized within a minute of time. The synthesized CuNCs was successfully utilized as a fluorescent probe to detect Hg^{2+} and S^{2-} ions. Importantly, we have prepared a smartphone aided paper-based kit for on-site monitoring of Hg^{2+} and S^{2-} ions.

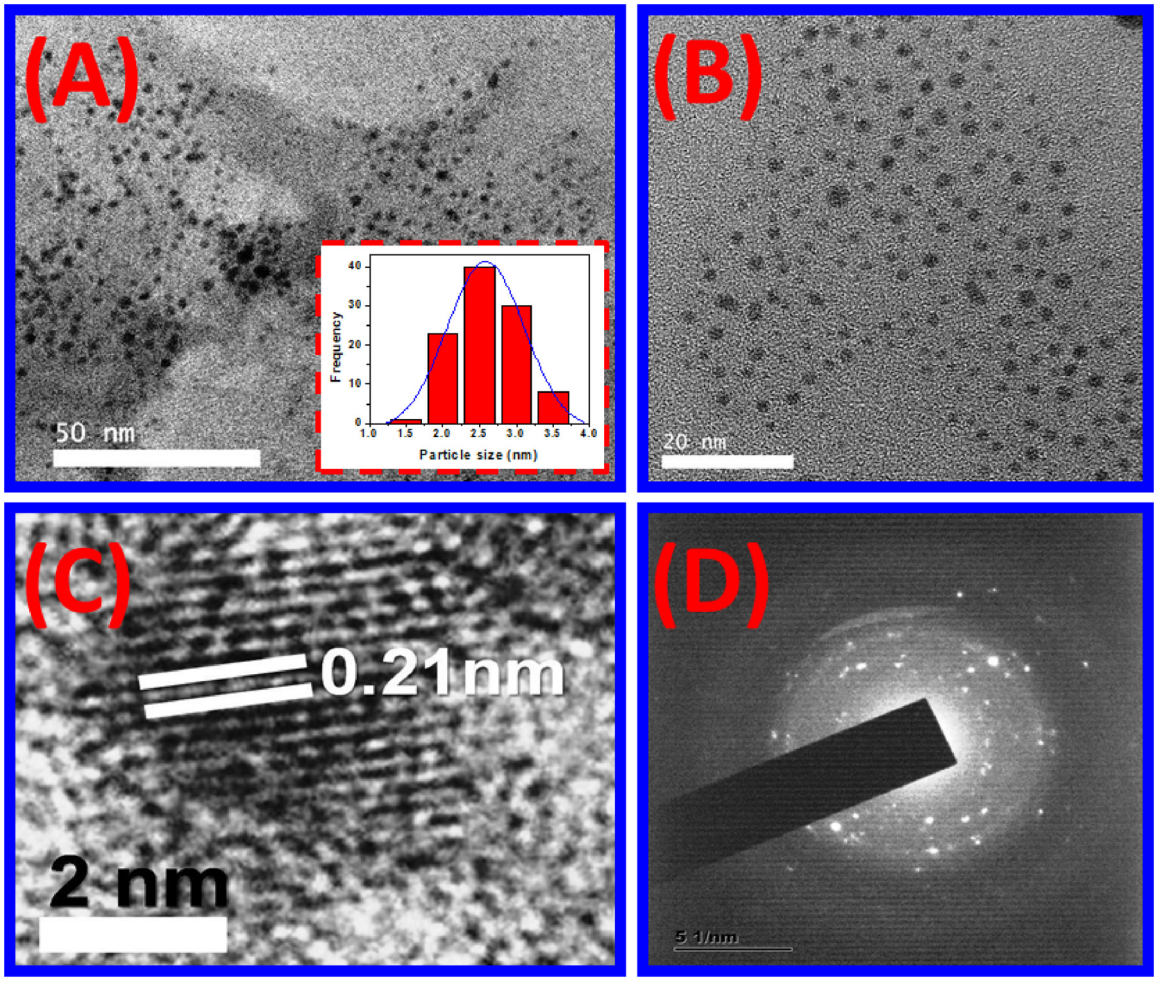

Fig. 2. HR-TEM images of TG-CuNCs with (A) 50 nm and (B) 20 nm scale magnifications. Inset A: Particle size histogram. (C) HR-TEM of the image of TG-CuNC, (D) Selected area diffraction pattern of TG-CuNCs.

2. Experimental section

2.1. Chemicals

1-Thio-β-D-glucose, ascorbic acid, and $Cu(NO_3)_2.3H_2O$ were obtained from Sigma-Aldrich and used without any purification. Sodium acetate, sodium fluoride, potassium chloride, sodium sulfate, potassium iodide, sodium chloride, lead nitrate, cadmium chloride, potassium bromide, potassium thiocyanate and quinine sulfate obtained from Sigma-Aldrich and used as received. Magnesium acetate, iron (III) chloride, cobalt nitrate, sodium nitrate, ammonium cyanide, sodium nitrite, nickel sulfate, iron (II) chloride, sodium hydroxide, zinc sulphate, manganese sulphate, mercury nitrate, $Na_2S.9H_2O$, Na_2HPO_4, H_2NaPO_4, EDTA, hydrochloric acid, sulfuric acid and nitric acid purchased from Fisher. Phosphate buffer solution (pH 3.0–13.0) was prepared by using Na_2HPO_4 and H_2NaPO_4 (0.2 M), the pH was adjusted by sodium hydroxide and hydrochloric acid. Glassware was washed with aqua-regia and rinsed with ultra-pure water.

2.2. Synthesis of TG-CuNCs

We have synthesized TG-CuNCs as follows. Briefly, 2 mL $Cu(NO_3)_2.3H_2O$ (10 mM) and 2.5 mL of ascorbic acid (25 mM) were added into a 25 mL beaker. Then, 1 mL of 100 mM, 1-Thio-β-D-glucose was added. Finally, 0.25 mL of 0.5 M NaOH was added into the above mixture was ultrasonicated 200 W, 40 ± 3 kHz for 26° C for 1 min. Then, the yellow solution was obtained. The synthesized 1-Thio-β-D-glucose capped copper nanocluster (TG-CuNCs) the resultant solution was centrifuge with 1000 rpm for 30 min. Then, the precipitate was redisposed with 20 mL of water solution was stored at 4° C.

2.3. Characterization of TG-CuNCs

Absorption spectral data were recorded in a Perkin Elmer Lambda 25 UV–vis spectrophotometer. Emission spectral data were recorded in a Perkin Elmer lambda LS45 spectrofluorometer. Fourier transform infrared (FT-IR) spectral data were collected from Fourier Transform Infrared spectrophotometer (JASCO 6300). Transmission electron microscopy (TEM) images and EDX (energy dispersive X-ray) spectrum were performed in a JEOL-2100 transmission electron microscopy and operated at 200 kV. XRD pattern was performed in a Rigaku X-ray diffraction unit using Ni-filtered CuK (λ = 1.54). Copper ions concentration was measured by the Inductively Coupled Plasma Mass Spectrometry (Agilent 7800 ICP-MS, USA). Digital images were acquired with the camera (13 + 5 dual megapixels) of a Lenovo K8 Note smartphone, equipped with Android 7.1.1, using the App Color Grab 3.6.1. The synthesis was carried out by Labman (LMUC-2) 200 W, 40 ± 3 kHz digital ultrasonic cleaner.

2.4. ICP-MS analysis

The total content of Cu^{2+} in the TG-CuNCs was determined by Inductively Coupled Plasma Mass Spectrometry (Agilent 7800 ICP-MS, USA). Before ICP-MS analysis, samples were microwave digested by

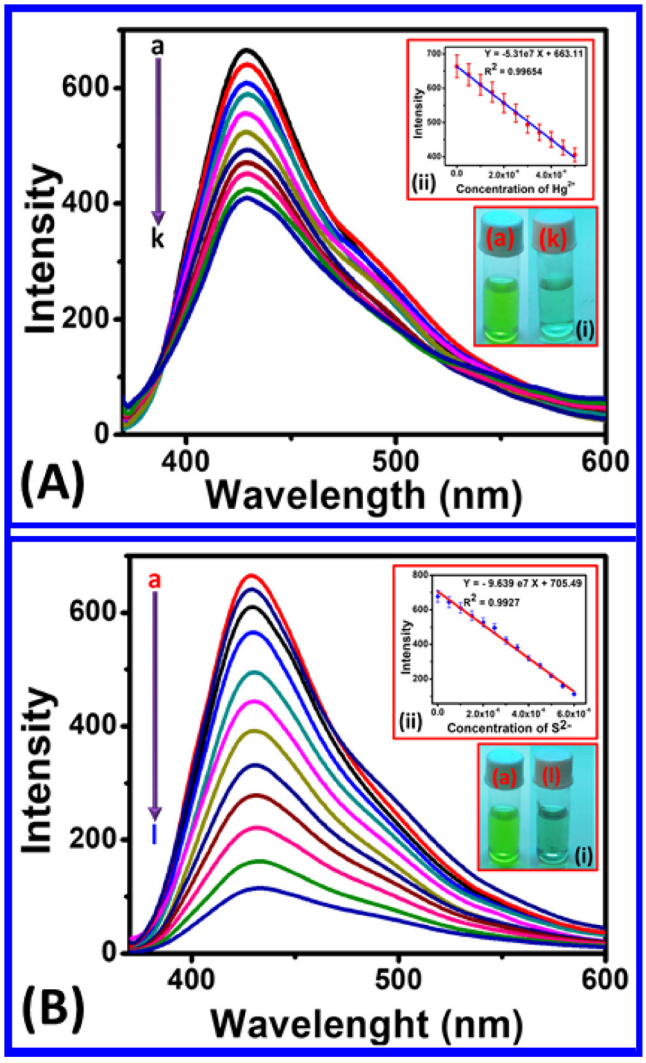

Fig. 3. (A) Emission spectra of TG-CuNCs in the presence of different concentration Hg^{2+} (a) 0, (b) 0.5, (c) 1.0, (d) 1.5, (e) 2.0, (f) 2.5, (g) 3.0, (h) 3.5, (i) 4.0, (j) 4.5 and (k) 5.0×10^{-6} M Hg^{2+}. Inset: (i) Photographs of (a) before and (k) after the addition of 5.0×10^{-6} M of Hg^{2+} and (ii) correlation line curve. (B) Emission spectra of TG-CuNCs in the presence of different concentration S^{2-} (a) 0, (b) 0.5, (c) 1.0, (d) 1.5, (e) 2.0, (f) 2.5, (g) 3.0, (h) 3.5, (i) 4.0, (j) 4.5, (k) 5.0 and (i) 5.5×10^{-6} M S^{2-}. Inset: (i) Photographs of (a) before and (k) after the addition 5.5×10^{-6} M of S^{2-} and (ii) correlation line curve. (For interpretation of the references to colour in this figure text, the reader is referred to the web version of this article.)

using a Discover SPD oven (CEM Corporation, Matthews, NC, USA). In a 25 mL glass vial, a known volume of TG-CuNCs was added and 5 mL of aqua regia (HNO_3/HCl = 1:3) was added and them for digession 12 h and made up to the known volume with ultrapure water. Afterwards, the samples were cooled down for 30 min at room temperature and made up to the known volume with ultrapure water. After appropriate dilutions, samples were analyzed by ICP-MS.

2.5. Sulfide and mercury ions sensor

0.5 mL of TG-CuNCs (Cu^{2+} ions concentration: 1.28 mg/L) and 1.5 mL of phosphate buffer (0.2 M; pH: 7) solution was taken (Blank) in a 3 mL cuvette. In this cuvette solution, a different concentration of Hg^{2+} or S^{2-} was added. After 3 and 5 min reaction time, absorption and fluorescence spectra were recorded for Hg^{2+} and S^{2-}, respectively. We kept 350 nm as an excitation wavelength for all the fluorescence spectral studies.

2.6. Quantum yield calculation

The Quantum Yield (QY) of TG-CuNCs, CuNCs-Hg(II) complex and sulfide adduct was determined through comparison of the wavelength-integrated intensity of the unknown sample with a standard. Quinine sulphate was used as the reference QY standard (QY = 0.54) (Melhuish, 1961). For this purpose, the fluorescent quantum yield value (ϕF) of TG-CuNCs and CuNCs-Hg(II) complex and sulfide adduct was calculated by using William's comparative method. The ϕF value was calculated according to the following equation:

$$QYx = \frac{Fx \times As \times QYs}{Fs \times Ax} \quad (1)$$

where, "Fx" is the integrated fluorescence emission of TG-CuNCs, "Fs" is the integrated fluorescence emission of the standard (Quinine sulphate), "Ax" is the absorbance at the excitation wavelength of TG-CuNCs, "As" is the absorbance at the excitation wavelength of the standard (Quinine sulphate), "QYx" is the quantum yield of TG-CuNCs, and "QYs" is the quantum yield of the standard fluorophore (Quinine sulphate QY = 0.54) (Melhuish, 1961).

2.7. Real sample analysis

Pond and river water was collected from nearby water resources. Tap water was taken from our institute. The dust and small particles were removed by simple filtration using Whatman filter paper No. 1. Then, we have spiked the known volume of real samples into TG-CuNCs and recorded the fluorescence spectra.

2.8. Preparation of smartphone aided paper-based kit

Whatman filter paper No.1 was cut into (1 × 2 cm) size pieces. Then, 100 µL of TG-CuNCs was added into each (1 × 2 cm) Whatman filter paper and dry at room temperature. Then, a known volume of real samples Hg^{2+} or S^{2-} was spiked on TG-CuNCs coated (1 × 2 cm) filter paper.

The on-site monitoring kit box was prepared by using waste PVC pipe (2 × 4 cm) and sample-hold cap (2 cm). UV-LED (5 mm; 395 – 400 nm) and carbon resistance (1.5 k ohm) was attached on the pipe, and the USP pin was connected. The TG-CuNCs coated filter paper (Blank) was placed into a kit box and USB was connected with a smartphone. Immediately, the UV-LED light shine and the fluorescent image was captured by a smartphone camera. Similarly, real samples added filter paper and Hg^{2+} or S^{2-} spiked filter paper image also captured by smartphone ((13 + 5 dual megapixels) of a Lenovo K8 Note). The captured images were uploaded into a Color Grab 3.6.1 App, the RGB-G color value was obtained. Based on the RGB-G color value the concentration of Hg^{2+} and S^{2-} was calculated using Microsoft excel app in a smartphone.

3. Results and discussion

3.1. Synthesis and characterization of TG-CuNCs

The TG-CuNCs was successfully synthesized by environmental and eco-friendly method at room temperature. TG-CuNCs was formed by ultrasonication within a min of time. Then, we have centrifuge the solution with 1000 rpm for 30 min. The purified TG-CuNCs was characterized by the following techniques.

3.2. Absorption and emission spectral studies and stability of TG-CuNCs

The synthesized TG-CuNCs exhibits the characteristic peaks at 252 and 300 nm (Fig. 1A; curve a), which are confirmed that the successful formation of TG-CuNCs (Vázquez-Vázquez et al., 2009). The emission spectrum of TG-CuNCs shows the maximum at 430 nm (excitation

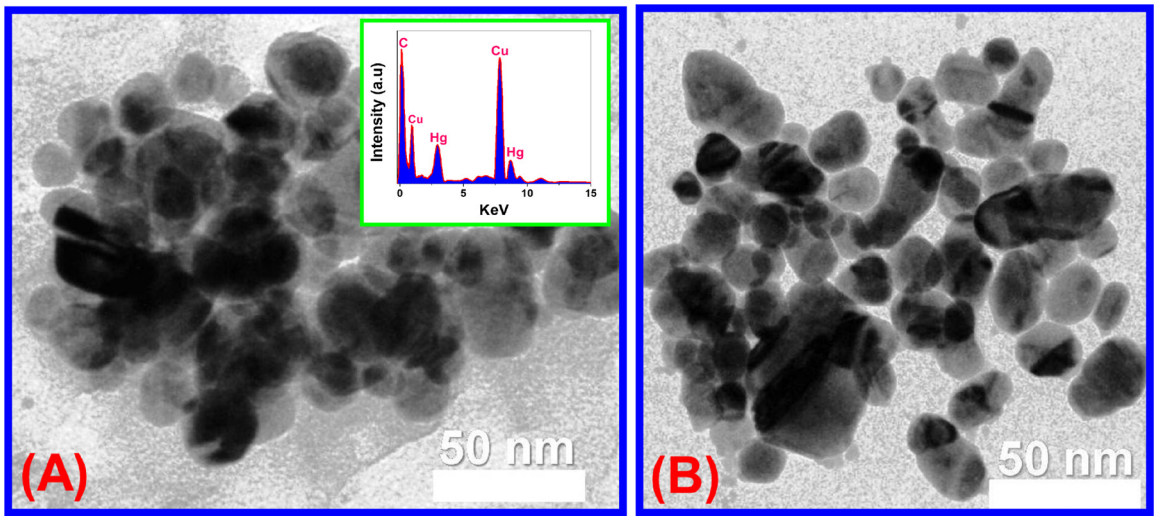

Fig. 4. HR-TEM images of TG-CuNCs in the presence of 5 μM concentration of Hg^{2+}. Inset: (A) EDX spectrum of TG-CuNCs in the presence of 5.0 μM of Hg^{2+}.

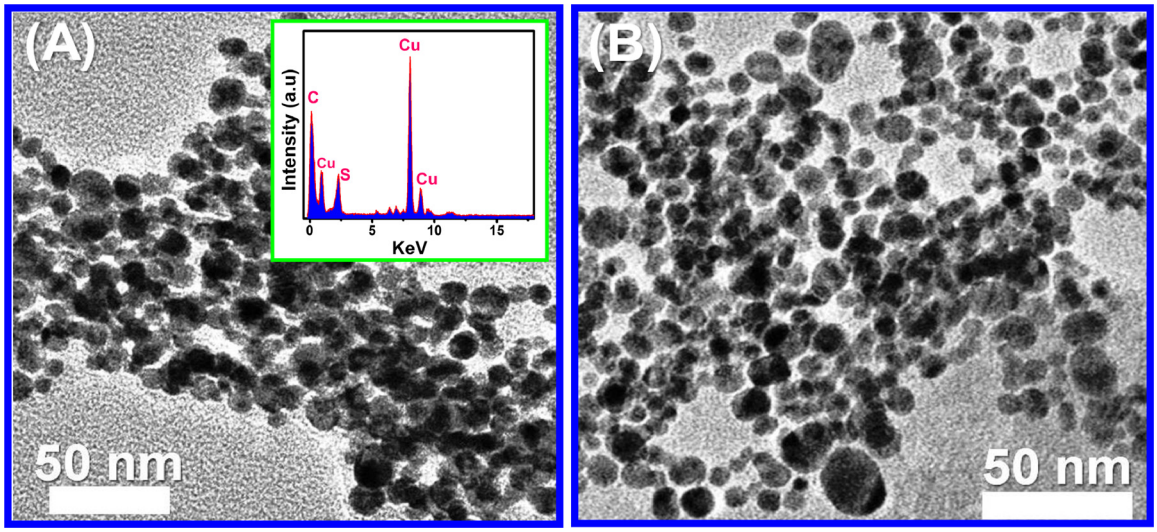

Fig. 5. HR-TEM images of TG-CuNCs in the presence of 5.5 μM concentration of S^{2-}. Inset: (A) EDX spectrum of TG-CuNCs in the presence of 5.5 μM of S^{2-}.

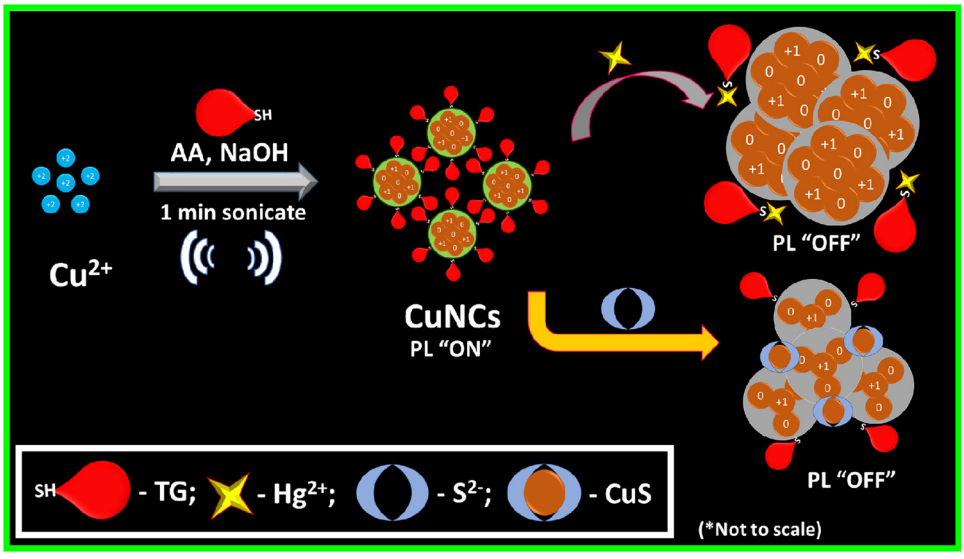

Scheme 1. Schematic representation for the possible mechanism of Hg^{2+} and S^{2-} detection using TG-CuNCs.

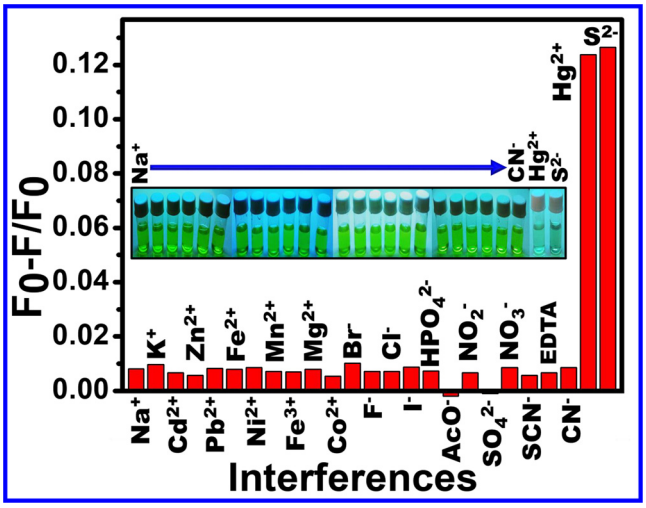

Fig. 6. Effect of Interferences: 1.08×10^{-3}M (720-fold) of Na^+, K^+, Cd^{2+}, Zn^{2+}, Pb^{2+}, Fe^{2+}, Ni^{2+}, Mn^{2+} and 9.0×10^{-4} M (600-fold) of Fe^{3+}, Mg^{2+}, Co^{2+} and 1.844×10^{-3} M (1229-fold) of Br-, F^-, Cl^-, I^-, $HPO_4{}^-$, AcO^-, $NO_2{}^-$, $SO_4{}^{2-}$, $NO_3{}^-$, SCN^-, EDTA, CN- and 1.5×10^{-6}M of Hg^{2+} and S^{2-}. Inset: Corresponding photographs.

Table 1
Real sample analysis for the detection of Hg^{2+}.

	Tap water		River water		Pond water	
Hg^{2+} spiked μM	Hg^{2+} found μM	Recovery %	Hg^{2+} found μM	Recovery %	Hg^{2+} found μM	Recovery%
-	0	-	0	-	0	-
1	1.014	101.4 ± 0.3	0.985	98.5 ± 0.2	0.987	98.7 ± 0.4
2	1.995	99.8 ± 0.2	2.013	101 ± 0.2	1.994	99.7 ± 0.3

Table 2
Real sample analysis for the detection of S^{2-}.

	Tap water		River water		Pond water	
S^{2-} spiked μM	S^{2-} found μM	Recovery %	S^{2-} found μM	Recovery %	S^{2-} found μM	Recovery %
-	0	-	0	-	0	-
1	1.01	101 ± 0.2	0.998	99.8 ± 0.2	0.994	99.4 ± 0.2
2	1.98	99 ± 0.4	1.991	99.6 ± 0.3	1.98	99 ± 0.3

wavelength: 350 nm) (Fig. 1A; curve b). Inset of 1A: (i) and (ii), corresponding photographs under day and UV-light (365 nm).

The formation of TG-CuNCs was monitored by UV–vis spectrophotometer and compared with their starting materials. The UV–vis spectrum of $Cu(NO_3)_2$ shows an absorption peak at 210 nm (Fig. S1 (A); curve a). Ascorbic acid absorption band was observed at 260 nm (Fig. S1 (A); curve b). $Cu(NO_3)_2$ and ascorbic acid mixture shows the absorption peak at 255 nm (Fig. S1 (A); curve c). On the other hand, TG shows the characteristic absorption peak at 222 nm (Fig. S1 (A); curve d). The mixture of $Cu(NO_3)_2$, ascorbic acid and TG exhibit the absorption peak at 262 nm (Fig. S1 (A); curve e). Interestingly, the synthesized TG-CuNCs absorption bands were observed at 252 and 300 nm (Fig. S1 (A); curve f), which is confirmed that the there is no excess of starting materials present in TG-CuNCs. Fig. S1 (B and C) shows the photographs of corresponding curves (a–f) under daylight and UV-light, respectively Among all, TG-CuNCs only have shown the green emission. These results are further revealed that the successful formation of fluorescent TG-CuNCs.

The stability of TG-CuNCs was monitored by UV–vis spectrophotometer. Surprisingly, 2-months aged and freshly prepared TG-CuNCs was un-altered with their absorbance and wavelength (Fig. 1B; curve a, b) and there are no color changes were observed (Fig. 1B; Inset i, ii). This result is confirmed that the synthesized TG-CuNCs are stable for 2-months.

3.3. FT-IR spectra of TG and TG-CuNCs

The chemical functional groups of TG and TG-CuNCs were characterized by FT-IR technique. FT-IR spectra of TG and TG-CuNCs are shown in Fig. 1C. The FT-IR spectrum of TG shows (Fig. 1C, curve a) the characteristic peaks at 3428 and 2922 cm^{-1}, which are corresponding stretching frequencies (ν) of OH, symmetrical stretching frequencies (ν_s) of CH (Smith, 2017; Watanabe et al., 2005). The stretching frequency (ν) of SH was observed at 2503 cm^{-1} (Farrell et al., 2017). The stretching frequency peak of C—O was observed at 1626 cm^{-1} (Smith, 2017; Geng et al., 2011). The stretching frequencies of CH and C—O—C were observed at 1345 and 1055 cm^{-1}, respectively (Smith, 2017; Maruthupandi et al., 2019).

The FT-IR spectrum of TG-CuNCs exhibits the similar FT-IR characteristic peaks of TG (Fig. 1C, curve b). It is expected that -SH group of TG adsorbed on the surface of CuNCs. As we expected that the resolved -SH peak intensity was decreased. This result is confirmed that the presence of TG on the surface of CuNCs.

3.4. XRD pattern and HR-TEM images of TG-CuNCs

Fig. 1D shows the XRD pattern of TG-CuNCs. We have observed the broad peak at 23°θ (Fig. 1D). The obtained peak value is perfectly matched with a previous report (Feng et al., 2017; Ghosh et al., 2014).

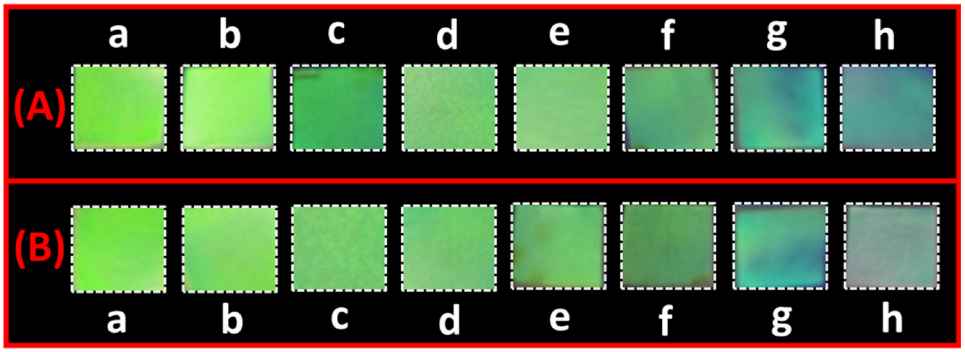

Fig. 7. (A) TG-CuNCs modified filter paper with the addition of (a) 0, (b) 0.25, (c) 0.5, (d) 1.0, (e) 1.5, (f) 2.5, (g) 3.5, (h) 4.5×10^{-6} M Hg^{2+} in pond water. (B) TG-CuNCs modified filter paper with the addition of (a) 0, (b) 0.25, (c) 0.5, (d) 1.0, (e) 1.5, (f) 2.5, (g) 3.5, (h) 4.5×10^{-6} M S^{2-} in pond water.

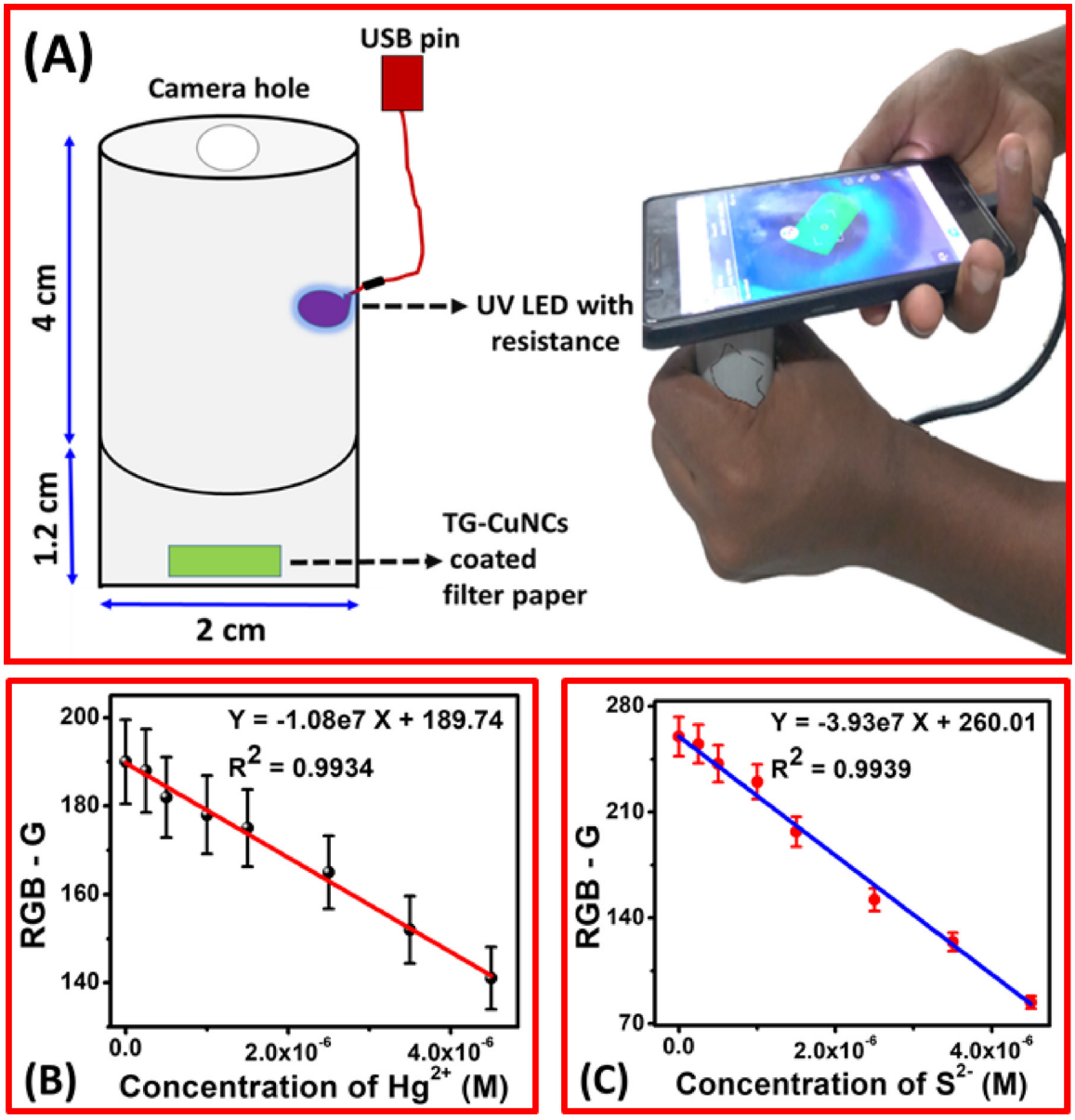

Fig. 8. (A) Schematic representation for the paper-based kit. (B) Correlation plot for linearity of RGB-G Vs concentration of Hg^{2+}. (C) Correlation plot for linearity of RGB-G Vs concentration of S^{2-}.

Further, we did not observe any characteristic plane of copper oxide and copper nanoparticles. This result is clearly confirmed that the lack of crystallinity of synthesized TG-CuNCs is ultra-small atomic size clusters (Feng et al., 2017; Ghosh et al., 2014). Transmission electron microscopy is an important technique to characterize the nanoparticles shape, size, dispersity and crystallinity. Fig. 2, illustrates the HR-TEM image of TG-CuNCs with different magnifications. Uniformly particles are dispersed and the average particles size was calculated to be 2.58 ± 0.03 nm by HR-TEM image (Fig. 2C) using particles size histogram (Fig. 2A; Inset) (Cao et al., 2014; Wang et al., 2015). Further, we have to measure the lattice distance from the single CuNC, which was calculated to be 0.21 nm (Miao et al., 2015; Ghosh et al., 2015). Moreover, the selected area diffraction pattern (SAED) also show that several rings. This result confirmed that the synthesized TG-CuNCs are crystalline nature (Fig. 2D). Furthermore, the obtained lattice distance value is perfectly match with the value previous reported (Jayasree et al., 2018). Further, the obtained precious ultra-small size TG-CuNCs (2.58 ± 0.03 nm) are clearly confirmed that the formation of copper nanoclusters (Cao et al., 2014; Wang et al., 2015). Importantly, we have calculated the quantum yield of TG-CuNCs and the details are given in the experimental Section 2.6. The quantum yield of TG-CuNCs was calculated to be 16.2 %.

3.5. Effect of pH and Time

The effect of pH with TG-CuNCs with Hg^{2+} and S^{2-} was monitored by fluorescence technique using phosphate buffer solution (Fig. S2 (A, B)). The pH of the Hg^{2+} and S^{2-} solutions was adjusted from 3 to 12, and then 1.5×10^{-6} M Hg^{2+} and S^{2-} was added and changes in the fluorescence intensity were examined. The fluorescence intensities were low at acidic pH (3–6) but the fluorescence intensity has reached a maximum at pH 7. Beyond pH 7 the fluorescence intensity was quenched (pH 8–12) (Fig. S2 (A, B)). The observed highly fluorescence intensity at pH 7, is due to the stability of TG and CuNCs at pH 7. In acidic pH, CuNCs will not be stable and formed Cu^{2+} ions. Whereas basic pH, particles get aggregation due to the excess of −OH ions. Therefore, we kept pH 7 for further studies.

On the other hand, it is very important to optimize the interaction

Table 3
Comparison of the sensitivity, LOD, sensing pH, real samples and limitation of the reported probes with TG-CuNCs probe for Hg^{2+} and S^{2-} sensing.

Materials	Linear Range (μM)	Sensing pH	LOD (nM) Hg^{2+}	LOD (nM) S^{2-}	Real Samples	Limitations	Ref.
DNA-functionalized gold nanoparticles	0.05–2.5	8.2	25	–	Pond water	Use of DNA, 16 h reaction time	Liu et al. (2008)
Carbon nanodots	0–3	8.5	4.2	–	Lake, tap and mountain water	400 °C for 2 h reaction time	Zhou et al. (2012)
Graphene quantum dots	0.6–12	6.5–8.5	230	–	Tap and pond water	16 h reaction time, higher LOD	Liu et al. (2015)
GSH capped CuNCs	0.04–60	8	22	–	Tap, lake and river water	85 °C for 7 h reaction time	Luo et al. (2017)
$NaYF_4$:Yb^{3+}/Er^{3+} nanophosphors and CdTeS QDs	0.01–2.8	7.4	15	–	Serum	200 °C for 2 h reaction time and long synthesis procedure	Cui et al. (2015)
OPDA-Carbon dots	30–60	7	60	–	–	180 °C for 5 h reaction time	Li et al. (2019)
N- Carbon dots	0.1–5	7.4	19	–	Tap and river water	160 °C for 6 h reaction time	Liao et al. (2019)
CTAB-CuNPs	12–50	10	–	8100	Tap and river water	80 °C for 45 min reaction time, higher LOD	Hatamie et al. (2014)
DNA-Ag/AuNDs	0.01–9	5	–	0.83	Hot spring and seawater	Use of DNA, acidic pH	Chen et al. (2011)
BSA-AuNCs	0.1–30	7	–	29	River water	Use of proteins 37 °C for 12 h reaction time	Cui et al. (2013)
Trypsin-AuNCs	0.5–8	9	–	5.5	Tap and river water	Use of enzymes 37 °C for 12 h reaction time	Fan et al. (2014)
Ce(III)/AgNCs complex	0.1–3.5	7	–	15	Tap and waste water	Using $NaBH_4$ toxic reducing agent, 7 days reaction time	Liu et al. (2019b)
Carbon dots/MnO2	2–25	6.5	–	800	Waste water	8 h reaction time, response time 50 min	Liu et al. (2019c)
TG-CuNCs	0.5–5.0, 0.5–5.5	7.0	1.7	1.02	Tap, river and pond Water	**Merits:** 1 min synthesis at Room temperature Neutral pH sensing medium Low LOD Response time: 3 and 5 min Smartphone aided paper-based kit was developed	This work

time TG-CuNCs with Hg^{2+} and S^{2-}. We have taken TG-CuNCs and add 1.5 μM Hg^{2+} then their fluorescence intensity changes were monitored with a different time interval (0 − 60 min). After the addition 1.5 μM Hg^{2+} into TG-CuNCs, the relative fluorescent intensity (F_0-F/F_0) was enhanced from 1 to 3 min (Fig. S3 (A)). Where "F_0" is the fluorescent intensity of TG-CuNCs and "F" is the fluorescent intensity of TG-CuNCs in the presence of 1.5×10^{-6} M Hg^{2+} or S^{2-}. From 5 to 60 min, the relative fluorescent intensity was constant.

Similarly, the addition of 1.5 μM S^{2-} into TG-CuNCs was led to increasing the relative fluorescence intensity from 1 to 5 min (Fig. S3 (B)), then it was remain constant. Finally, we have concluded that 3 and 5 min are optimal for the interaction of TG-CuNCs with Hg^{2+} and S^{2-}, respectively. Therefore, we kept 3 and 5 min for the reaction time and pH 7 maintained for Hg^{2+} and S^{2-}, respectively, for further studies.

3.6. Spectrophotometric and spectrofluorometric detection of Hg^{2+} ions

The absorption spectrum of TG-CuNCs exhibits the peaks at 252 and 300 nm (Fig. S4 (A); Curve a). After the addition of 0.5 μM concentration Hg^{2+} absorbance peak at 252 was increased and peak 300 was decreased. Interestingly, one new peak appeared at 218 nm (Fig. S4 (A); Curve b–h). The observed changes are due to the interaction of Hg^{2+} with TG ligand (-SH and −OH groups) and led to the aggregation of copper nanoclusters (Fig. S4 (A)) (Shigemoto et al., 2019; Vasimalai et al., 2012).

It is well known that fluorescence technique is more sensitive than the absorption studies. Therefore, we made an attempt to sense Hg^{2+} by fluorescence technique. The emission spectrum of TG-CuNCs excited the emission maximum at 430 nm (Fig. 3A; Curve a). After the addition of 0.5 μM concentration of Hg^{2+} the fluorescence of TG-CuNCs was quenched (Fig. 3A; Curve b). Then, 1.0–5.0 μM concentration of Hg^{2+} also decreased the fluorescence of TG-CuNCs at 430 nm (Fig. 3A; Curve c–k). The color of the solution was changed from green to colorless under UV irradiation (Fig. 3A; Inset i). It is expected that the observed color and spectral changes may be due to the aggregation of copper nanoclusters. The good linearity was observed from 500 nM to 5 μM concentration of Hg^{2+}. Based on the decreases in fluorescence intensity, the detection limit was calculated to be 1.7 nM (LOD = 3S/m) (Fig. 3A; Inset ii). Moreover, we have calculated the quantum yield of TG-CuNCs with the different concentration addition of Hg^{2+} which was found to be 7.0 %. The observed 2.28-fold decreases of quantum yield, is expected due to the aggregation of TG-CuNCs through the intraction between TG-CuNCs and Hg^{2+} ions.

3.7. Spectrophotometric and spectrofluorometric detection of S^{2-} ions

UV-vis spectrum of TG-CuNCs peaks is observed at 252 and 300 nm (Fig. S4 (B); Curve a). After the addition of 0.5 μM concentration S^{2-} absorbance peak 300 nm was shifted to 341 nm (Fig. S4 (B); Curve b–i). The observed peak at 211 nm (Fig. S4 (B); Curve b) was attained to the red shift with the increases in absorbance (Fig. S4 (B); Curve c–i) while add the different concentration of S^{2-}. It is also expected that the absorbance increases at 341 nm is due to the formation of copper(II) complex (CuS) (Hatamie et al., 2014; Cao et al., 2011; Wen et al., 2019).

The emission spectrum of TG-CuNCs exhibited the emission maximum at 430 nm (Fig. 3B; Curve a). After the addition of 0.5 μM concentration of S^{2-} also was led to a decrease in the fluorescence of TG-CuNCs (Fig. 3B; Curve b). Then, the addition from 1.0 to 5.5 μM concentration of S^{2-} also decreased the fluorescence of TG-CuNCs at 430 nm (Fig. 3B; curve c–l). The green color solution was changed to pale-brown under UV irradiation (Fig. 3B; Inset i). It is expected that the observed color and spectral changes may be due to the aggregation of copper nanoclusters and the formation of CuS complex. Based on the decreases in fluorescence intensity, the limit of detection was calculated to be 1.02 nM (LOD = 3S/m). The good linearity was observed 500 nM

to 5.5 μM (Fig. 3B; Inset ii). Moreover, we have calclulated the quantum yield of TG-CuNCs after the adttion different concentration of S^{2-}, which was found to be 6.6 %. The observed 2.42-fold decreases of quantum yield, is expected due to the aggregation TG-CuNCs, through the complex formation.

3.8. HR-TEM of TG-CuNCs in the presence of Hg^{2+} and S^{2-} ions

Fig. 4 shows the TEM image of TG-CuNCs in the presence of 5 μM concentration of Hg^{2+}. This image shows the aggregated particles structure. The aggregated nanoparticles size was calculated to be ~ 30 nm. The observed aggregation is expecting due to the interaction between -SH group of TG ligand and Hg^{2+}. It is well known that Hg^{2+} has a strong thiophilic tendency with -SH group. Therefore, CuO did not form (Dutta et al., 2015). Hence, it led to aggregate the nanoparticles (Shigemoto et al., 2019; Vasimalai et al., 2012). Moreover, we have taken EDX spectrum of TG-CuNCs in the presence of 5.0 μM of Hg^{2+}, which is shown in the inset of Fig. 4A. The EDX spectrum revealed the strong signals of copper at 7.83 KeV and mercury at 2.92 and 8.71 KeV. These results confirmed the formation of thiol-Hg^{2+} complex. Further, these results are perfectly match with the previous reports (Abdulla-Al-Mamun et al., 2010; Li et al., 2010).

On the other hand, TEM images of TG-CuNCs in the presence of 5.5 μM of S^{2-} shows the aggregated structure nanoparticles (Fig. 5). The aggregated particles size was calculated to be~ 17 nm. The observed aggregation may be due to the formation of CuS (Hatamie et al., 2014; Cao et al., 2011; Wen et al., 2019). Moreover, we have measured the EDX spectrum of TG-CuNCs in the presence of 5.5 μM of S^{2-} (Inset of Fig. 5A). The EDX spectrum of TG-CuNCs in the presence of 5.5 μM of S^{2-} revealed that the strong signals of sulfide at 2.3 KeV and copper at 8.09 KeV. Further, these results perfectly match with previous reports (Abdulla-Al-Mamun et al., 2010; Gautam et al., 2014).

3.9. Quenching constant and detection mechanism

Quenching constant of TG-CuNCs was calculated using Eq. (2), (Vasimalai et al., 2018)

$$\frac{F0}{F} = 1 + KSV\,[Q] \tag{2}$$

where, ``F`` and ``$F_0$`` are the fluorescence intensities of TG-CuNCs at 430 nm in the presence and absence of Hg^{2+} or S^{2-}, respectively ``$K_{SV}$`` is the quenching constant. "[Q]" is the Hg^{2+} or S^{2-} concentration. The quenching constant (Hg^{2+}) was calculated to be $1.324 \times 10^5\ M^{-1}$. The positive deviated curve that was obtained is due to the presence of both static and dynamic quenching for Hg^{2+} (Fig. S5 (A)). On the other hand, the positive deviated curve that was obtained is due to the simultaneous presence of dynamic and static quenching for S^{2-} (Fig. S5 (B)). The quenching constant (S^{2-}) was calculated to be $3.39 \times 10^5\ M^{-1}$.

Schematic representation of the possible mechanism for the detection of Hg^{2+} and S^{2-}. The green emission TG-CuNCs we have the interaction of TG-ligand and Hg^{2+} from the complex which let to aggregation the nanoclusters (Scheme 1) (Shigemoto et al., 2019; Vasimalai et al., 2012) and other hands hence S^{2-} can from CuS let to aggregation (Scheme 1) (Hatamie et al., 2014; Cao et al., 2011; Wen et al., 2019). Finally, we have confirmed that mechanism based on the UV–vis, fluorescent and TEM.

3.10. Effect of interferences

We have taken different cations and anions as potential interferences. Interestingly, 1.08×10^{-3}M (720-fold) of Na^+, K^+, Cd^{2+}, Zn^{2+}, Pb^{2+}, Fe^{2+}, Ni^{2+} and Mn^{2+} and 9.0×10^{-4} M (600- fold) of Fe^{3+},

Mg^{2+} and Co^{2+} and 1.844×10^{-3}M (1229-fold) of Br^-, F^-, Cl^-, I^-, HPO_4^-, AcO^-, NO_2^-, SO_4^{2-}, NO_3^-, SCN^-, EDTA, CN^- interference did not interfere to detect 1.5×10^{-6} M of Hg^{2+} and S^{2-}, respectively (Fig. 6). No color changes were observed in the above-mentioned interferences (under UV light (365 nm), (Fig. 6: Inset). But, 1.5 μM of Hg^{2+} or S^{2-} addition, the green fluorescence was quenched. These results are confirmed that the synthesized TG-CuNCs is highly selective for the detection of Hg^{2+} and S^{2-} in the presence of very high concentrations of above mentioned common interferences (Fig. 6).

We have taken S^{2-}: 20×10^{-6} M S^{2-} with 1.08×10^{-3} M of Cd^{2+} and Hg^{2+}: 20×10^{-6} M Hg^{2+} with 1.844×10^{-3} M EDTA use masking agent to mask (Fig. S6). Above stated common masking agent did not interfere for the detection of 1.5×10^{-6} M of Hg^{2+} and S^{2-}. Fig. S6: Inset corresponding photographs. Which are confirmed the masking agent to chelate the analyte and did not interfere for the detection of other analytes.

3.11. Real sample analysis

TG-CuNCs probe was effectively applied to detect Hg^{2+} and S^{2-} in tap, river and pound water samples (Tables 1 and 2). Hg^{2+} and S^{2-} was not initially detected in the tap, river and pond water samples. Then, we spiked a known amount of Hg^{2+} to the real samples, which led to the quench of the intensity. Good recovery was observed from 98.5 to 101.4 % of those spiked with Hg^{2+} (Table 1).

On the other hand, we spiked a known amount of S^{2-} to the real samples, which led to the quenching of the fluorescent intensity. Good recovery was observed from 99 to 101 % of those spiked with S^{2-} (Table 2). These results are revealed that TG-CuNCs probe had a good performance in terms of simplicity and precision of analysis of Hg^{2+} and S^{2-} in water samples.

3.12. Smartphone aided paper-based kit for the detection of Hg^{2+} and S^{2-}

We have prepared the smartphone aided kit from PVC waste pipe. The details of designing are given in the experimental Section 2.8. First, we have taken Whatman No:1 filter paper and cut into a small piece (1 × 2 cm). Then, TG-CuNCs was added on the top of the paper and details are given the experimental Section 2.8. The pond water sample of 20 μL containing known concentration from 0.25 to 4.5×10^{-6} M Hg^{2+} or S^{2-} was added. Then, the paper was allowed to dry at room temperature. Further, it was irradiated into UV-light. The green fluorescent in a paper was quanched (Fig. 7). The observed changes color was confirmed the particles aggregation. The same paper was used to detect the existing Hg^{2+} or S^{2-} by smartphone.

The paper was fixed into the bottom PVC pipe (1.2 cm size), then it was fixed with 4 cm PVC pipe. When we connect the USP pin with a smartphone. The UV-LED will be shine and image was captured by a smartphone camera (Fig. 8A). The captured image was uploaded into a color grab 3.6.1 app, then we have obtained the RGB-G color value. It shows the good linearity from 0.25 to 4.5 μM for Hg^{2+} and S^{2-} (Fig. 8B, C).

These results are confirmed that our smartphone aided paper-based kit provides advantage including low cost, good ability, test screening, a simple experimental step and on-site monitoring of Hg^{2+} and S^{2-} in different water samples (Table 3).

4. Conclusions

In this article, we have reported the one-minute synthesis of TG-CuNCs by ultrasonication. The synthesized TG-CuNCs are stable for more than 2 months and characterized by UV–vis, FT-IR, HR-TEM and XRD techniques. Then, we have used TG-CuNCs as a probe for the detection of Hg^{2+} and S^{2-} ions. The addition of Hg^{2+} or S^{2-} was led to quench the green fluorescence of TG-CuNCs under UV light (365 nm). A detection limit was calculated to be 1.7 and 1.02 nM for Hg^{2+} and S^{2-}, respectively. Even 600-fold of common interference did not interfere

with the detection of 1.5×10^{-6} M of Hg^{2+} and S^{2-} ions. We have applied the system for this detection of Hg^{2+} or S^{2-} in different tap, river and pond water samples. Importantly, we have developed a smartphone aided kit for on-site monitoring for Hg^{2+} and S^{2-}. This is the first report for the synthesis of CuNCs within min of time. This is a low-cost kit having a good ability, test screening, a simple experimental step and on-site monitoring. Finally, we have successfully validated with RGB-G app value. We strongly believe that the developed smartphone aided kit and synthesized TG-CuNCs will be a useful kit and material in the field of nanotechnology, environmental monitoring and material science.

Acknowledgements

Mr. M. Maruthupandi thanks to B.S. Abdur Rahman Crescent Institute of Science and Technology, Chennai-600 048, India for the award of Junior Research Fellow under the BSA-JRF University Fellowship (Lr. No. 773/ Dean (R) 2019/05.08.2019). Dr. N. Vasimalai greatly acknowledge to the B.S. Abdur Rahman Crescent Institute of Science and Technology, Chennai-600 048, India for grant of Crescent Seed money (Lr. No. 1242/ Dean (R) 2019/31.12.2019).

Appendix A. Supplementary data

Supplementary material related to this article can be found, in the online version, at doi:https://doi.org/10.1016/j.jhazmat.2020.122294.

References

Abdulla-Al-Mamun, M., Kusumoto, Y., Ahmmad, B., Shariful Islam, M., 2010. Photocatalytic cancer (HeLa) cell-killing enhanced with Cu–TiO_2 nanocomposite. Top. Catal. 53, 571–577.

Afkhami, A., Khalafi, L., 2005. Indirect determination of sulfide by cold vapor atomic absorption spectrometry. Microchim Acta 150, 43–46.

Aparna, R.S., Anjali Devi, J.S., Nebu, J., Syamchand, S.S., George, S., 2019. Rapid response of dopamine towards insitu synthesised copper nanocluster in presence of H_2O_2. J. Photochem. Photobiol. A 379, 63–71.

Bowen, H.J.M., 1979. Environmental Chemistry of the Elements. Academic Press, New York 1979.

Cao, X., Lin, W., He, L., 2011. A near-infrared fluorescence turn-on sensor for sulfide anions. Org. Lett. 13 (17), 4716–4719.

Cao, H., Chen, Z., Zheng, H., Huang, Y., 2014. Copper nanoclusters as a highly sensitive and selective fluorescence sensor for ferric ions in serum and living cells by imaging. Biosens. Bioelectron. 62, 189–195.

Cao, D., Liu, Z., Verwilst, P., Koo, S., Jangjili, P., Seung Kim, J., Lin, W., 2019. Coumarin-based small-molecule fluorescent chemosensors. Chem. Rev. 119 (18), 10403–10519.

Chen, W.Y., Lan, G.Y., Chang, H.T., 2011. Use of fluorescent DNA-templated gold/silver nanoclusters for the detection of sulfide ions. Anal. Chem. 83, 9450–9455.

Craig Cooper, D., Morse, J.W., 1998. Extractability of metal sulfide minerals in acidic solutions: application to environmental studies of trace metal contamination within anoxic sediments. Environ. Sci. Technol. 32, 1076–1078.

Cui, M.L., Liu, J.M., Wang, X.X., Lin, L.P., Jiao, L., Zheng, Z.Y., Zhang, L.H., Jiang, S.L., 2013. A Promising gold nanoclusters fluorescence sensor for highly sensitive and selective detection of S^{2-}. Sens. Actuators B 188, 53–58.

Cui, S., Xu, S., Song, H., Xu, W., Chen, X., Zhou, D., Yin, Z., Han, W., 2015. Highly sensitive and selective detection of mercury ions based on up-conversion FRET from $NaYF_4$: Yb^{3+}/Er^{3+} nanophosphors to CdTe quantum dots. RSC Adv. 5, 99099–99106.

Dilgin, Y., Kızılkaya, B., Ertek, B., Eren, N., Giray Dilgin, D., 2012. Amperometric determination of sulfide based on its electrocatalytic oxidation at a pencil graphite electrode modified with quercetin. Talanta 89, 490–495.

Dutta, B., Kar, E., Bosea, N., Mukherjee, S., 2015. Significant enhancement of the electroactive β-phase of PVDF by incorporating hydrothermally synthesized copper oxide nanoparticles. RSC Adv. 5, 105422–105434.

Erxleben, H., Ruzicka, J., 2005. Atomic absorption spectroscopy for mercury, automated by sequential injection and miniaturized in lab-on-valve system. Anal. Chem. 77, 5124–5128.

Fan, J., Li, R., Xu, P., Di, J., Tu, Y., Yan, J., 2014. Sensitive sulfide sensor with a trypsin-stabilized gold nanocluster. Anal. Sci. 30, 457–462.

Farrell, M.J., Reaume, R.J., Pradhan, A.K., 2017. Visual detection of denatured glutathione peptides: a facile method to visibly detect heat stressed biomolecules. Sci. Rep. 7, 2604.

Feng, J., Chen, Y., Han, Y., Liu, J., Ma, S., Zhang, H., Chen, X., 2017. pH-regulated synthesis of trypsin-templated copper nanoclusters with blue and yellow fluorescent emission. ACS Omega 2, 9109–9117.

Gautam, D., Nitul, K., Seok Hee, L., Niranjan, K., Young Soo, Y., 2014. Water soluble sodium sulfate nanorods as a versatile template for the designing of copper sulfide nanotubes. J. Nanosci. Nanotechnol. 14, 4455–4461.

Gedanken, A., 2004. Using sonochemistry for the fabrication of nanomaterials. Ultrason. Sonochem. 11, 47–55.

Geng, F., Song, K., Xing, J.Z., Yuan, C., Yan, S., Yang, Q., Chen, J., Kong, B., 2011. Thioglucose bound gold nanoparticles enhance radio-cytotoxic targeting of ovarian cancer. Nanotechnology 22, 285101 (8pp).

Ghosh, R., Sahoo, A.K., Ghosh, S.S., Paul, A., Chattopadhyay, A., 2014. Blue-emitting copper nanoclusters synthesized in the presence of lysozyme as candidates for cell labeling. ACS Appl. Mater. Interfaces 6, 3822–3828.

Ghosh, R., Goswami, U., Ghosh, S.S., Paul, A., Chattopadhyay, A., 2015. Synergistic anticancer activity of fluorescent copper nanoclusters and cisplatin delivered through a hydrogel nanocarrier. ACS Appl. Mater. Interfaces 71, 209–222.

Guenther, E.A., Johnson, K.S., Coale, K.H., 2001. Direct ultraviolet spectrophotometric determination of total sulfide and iodide in natural waters. Anal. Chem. 73, 3481–3487.

Hatamie, A., Zargar, B., Jalali, A., 2014. Copper nanoparticles: a new colorimetric probe for quick, naked-eye detection of sulfide ions in water samples. Talanta 121, 234–238.

Huang, C.C., Chang, H.T., 2006. Selective gold-nanoparticle-based "Turn-On" fluorescent sensors for detection of mercury(II) in aqueous solution. Anal. Chem. 78, 8332–8338.

Huang, H., Li, H., Feng, J.J., Wang, A.J., 2016. One-step green synthesis of fluorescent bimetallic Au/Ag nanoclusters for temperature sensing and in vitro detection of Fe^{3+}. Sens. Actuators B 223, 550–556.

Jayasree, M., Aparna, R.S., Anjana, R.R., Anjali Devi, J.S., John, N., Abha, K., Manikandan, A., George, S., 2018. Fluorescence turn on detection of bilirubin using Fe (III) modulated BSA stabilized copper nanocluster; a mechanistic perception. Anal. Chim. Acta 1031, 152–160.

Jung, M.C., 2001. Heavy metal contamination of soils and waters in and around the Imcheon Au–Ag mine. Korea. Appl. Geochem. 16, 1369–1375.

Kanchana, P., Sudhan, N., Anandhakumar, S., Mathiyarasu, J., Manisankar, P., Sekar, C., 2015. Electrochemical detection of mercury using biosynthesized hydroxyapatite nanoparticles modified glassy carbon electrode without preconcentration. RSC Adv. 5, 68587–68594.

Kang, J.H., Yang, M., Yun, D., Kim, M., Lee, H., Kim, K.T., Lim, M.H., Kim, C., 2019. A dual-response sensor based on NBD for the highly selective determination of sulfide in living cells and zebrafish. New J. Chem. 43, 4029–4035.

Li, W., Guo, Y., McGill, K., Zhang, P., 2010. A facile synthesis of Ag nanoparticles for mercury ion detection with high sensitivity and selectivity. New J. Chem. 34, 1148–1152.

Li, B., Ma, H., Zhang, B., Qian, J., Cao, T., Feng, H., Li, W., Dong, Y., Qin, W., 2019. Dually emitting carbon dots as fluorescent probes for ratiometric fluorescent sensing of pH values, mercury(II), chloride and Cr(VI) via different mechanisms. Microchim. Acta 186, 341.

Liang, M., Chen, Y., Zhang, H., Niu, X., Xu, L., Ren, C., Chen, X., 2015. Fluorescence resonance energy transfer-based ratiometric fluorescent assay for highly sensitive and selective determination of sulfide anion. Analyst 140, 6711–6719.

Liao, S., Li, X., Yang, H., Chen, X., 2019. Nitrogen-doped carbon dots rapid and selective detection of mercury ion and biothiol and construction of an IMPLICATION logic gate. Talanta 194, 554–562.

Lin, Q., Lu, T.T., Zhu, X., Wei, T.B., Li, H., Zhang, Y.M., 2016. Rationally introduce multi-competitive binding interactions in supramolecular gels: a simple and efficient approach to develop multi-analyte sensor array. Chem. Sci. 7, 5341–5346.

Lin, Q., Zhong, K.P., Zhu, J.H., Ding, L., Su, J.X., Yao, H., Wei, T.B., Zhang, Y.M., 2017a. Iodine controlled pillar[5]arene-based multiresponsive supramolecular polymer for fluorescence detection of cyanide, mercury, and cysteine. Macromolecules 50 (20), 7863–7871.

Lin, L., Hu, Y., Zhang, L., Huang, Y., Zhao, S., 2017b. Photoluminescence light-up detection of zinc ion and imaging in living cells based on the aggregation induced emission enhancement of glutathione-capped copper nanoclusters. Biosens. Bioelectron. 94, 523–529.

Lin, Q., Fan, Y.Q., Mao, P.P., Liu, L., Liu, J., Zhang, Y.M., Yao, H., Wei, T.B., 2018. Pillar[5]arene-based supramolecular organic framework with multi-guest detection and recyclable separation properties. Chem. Eur. J. 24, 777–783.

Liu, C.W., Huang, C.C., Chang, H.T., 2008. Control over surface DNA density on gold nanoparticles allows selective and sensitive detection of mercury(II). Langmuir 24, 8346–8350.

Liu, M., Liu, T., Li, Y., Xu, H., Zheng, B., Wang, D., Du, J., Xiao, D., 2015. A FRET chemsensor based on graphene quantum dots for detecting and intracellular imaging of Hg^{2+}. Talanta 143, 442–449.

Liu, J., Fan, Y.Q., Song, S.S., Gong, G.F., Wang, J., Guan, X.W., Yao, H., Zhang, Y.M., Wei, T.B., Lin, Q., 2019a. Aggregation-induced emission supramolecular organic framework (AIE SOF) gels constructed from supramolecular polymer networks based on tripodal pillar[5]arene for fluorescence detection and efficient removal of various analytes. ACS Sustain. Chem. Eng. 7, 11999–12007.

Liu, J., Bao, H., Ma, D.L., Leung, C.H., 2019b. Silver nanoclusters functionalized with Ce (III) ions are a viable Bturn-on-off fluorescent probe for sulfide. Microchim. Acta 186, 16.

Liu, J., Liu, C., Zhou, Z., 2019c. A turn-on fluorescent sulfide probe prepared from carbon dots and MnO_2 nanosheets. Microchim. Acta 186, 281.

Lu, Y., Chen, W., 2012. Sub-nanometre sized metal clusters: from synthetic challenges to the unique property discoveries. Chem. Soc. Rev. 41, 3594–3623.

Luo, T., Zhang, S., Wang, Y., Wang, M., Liao, M., Kou, X., 2017. Glutathione-stabilized Cu nanocluster-based fluorescent probe for sensitive and selective detection of Hg^{2+} in water. Luminescence 32 (6), 1092–1099.

Maruthupandi, M., Chandhru, M., Kutti Rani, S., Vasimalai, N., 2019. Highly selective detection of iodide in biological, food, and environmental samples using polymer-capped silver nanoparticles: preparation of a paper-based testing kit for on-site

monitoring. ACS Omega 4, 11372–11379.
Melhuish, W.H., 1961. Quantum efficiencies of fluorescence of organic substances: effect of solvent and concentration of the fluorescent solute. J. Phys. Chem. 65 (2), 229–235.
Miao, H., Zhong, D., Zhoub, Z., Yang, X., 2015. Papain-templated Cu nanoclusters: assaying and exhibiting dramatically antibacterial activity cooperating with H_2O_2. Nanoscale 7, 19066–19072.
Prodi, L., Bargossi, C., Montalti, M., Zaccheroni, N., Su, N., Bradshaw, J.S., Izatt, R.M., Savage, P.B., 2000. An effective fluorescent chemosensor for mercury ions. J. Am. Chem. Soc. 122, 6769–6770.
Rekhi, H., Rani, S., Sharma, N., Malik, A.K., 2017. A review on recent applications of high performance liquid chromatography in metal determination and speciation analysis. Crit. Rev. Anal. Chem. 47 (6), 524–537.
Shigemoto, A.K., Killjoy, A.A., Dayton, J., Virca, C.N., McCormick, T.M., 2019. Increased binding of thiophene-based ligands to mercury (II) with water solubilizing functional groups. Mol. Syst. Des. Eng. https://doi.org/10.1039/C9ME00055K. https://pubs.rsc.org/en/content/articlelanding/2020/me/c9me00055k#!divAbstract.
Smith, B.C., 2017. An IR spectral interpretation potpourri: carbohydrates and alkynes. Spectroscopy 32, 18–24.
Tang, D., Santschi, P.H., 2000. Sensitive determination of dissolved sulfide in estuarine water by solid-phase extraction and high-performance liquid chromatography of methylene blue. J. Chromatogr. A 883, 305–309.
Vaaramaa, K., Lehto, J., 2003. Removal of metals and anions from drinking water by ion exchange. Desalination 155, 157–170.
Vasimalai, N., Abraham John, S., 2015. Off-on and on-off chemosensors for ultratrace mercury(II) and copper(II) using functionalized thiazole and cadmium sulfide nanoparticles fluorophores. Sens. Actuators B 190, 800–808.
Vasimalai, N., Sheeba, G., Abraham John, S., 2012. Ultrasensitive fluorescence-quenched chemosensor for Hg(II) in aqueous solution based on mercapto thiadiazole capped silver nanoparticles. J. Hazard. Mater. 213 − 214, 193–199.
Vasimalai, N., Fernández-Argüelles, M.T., Espiña, B., 2018. Detection of sulfide using mercapto tetrazine protected fluorescent gold nanodots: the preparation of paper based testing kit for on-site monitoring. ACS Appl. Mater. Interfaces 10 (2), 1634–1645.
Vázquez-Vázquez, C., Bañobre-López, M., Mitra, A., Arturo López-Quintela, M., Rivas, J., 2009. Synthesis of small atomic copper clusters in microemulsions. Langmuir 25 (14), 8208–8216.
Wang, C., Shu, S., Yao, Y., Song, Q., 2015. A fluorescent biosensor of lysozyme-stabilized copper nanoclusters for the selective detection of glucose. RSC Adv. 00, 1–7.
Watanabe, S., Seguchi, H., Yoshida, K., Kifune, K., Tadaki, T., Shiozaki, H., 2005. Colorimetric detection of fluoride ion in an aqueous solution using a thioglucose-capped gold nanoparticle. Tetrahedron Lett. 46, 8827–8829.
Wen, Z., Song, S., Hu, T., Wang, C., Qu, F., Wang, P., Yang, M., 2019. A dual emission nanocomposite prepared from copper nanoclusters and carbon dots as a ratiometric fluorescent probe for sulfide and gaseous H_2S. Microchim. Acta 186 (258), 1–8.
WHO, 1996. Guidelines for Drinking-Water Quality: Health Criteria and Other Supporting Information, 2nd ed. WHO Publ. 2, Geneva, pp. 1–11.
Yuan, Z., Peng, M., Shi, L., Du, Y., Cai, N., He, Y., Chang, H.T., Yeung, E.S., 2013. Disassembly mediated fluorescence recovery of gold nanodots for selective sulfide sensing. Nanoscale 5, 4683–4686.
Zhou, L., Lin, Y., Huang, Z., Ren, J., Qu, X., 2012. Carbon nanodots as fluorescence probes for rapid, sensitive, and label-free detection of Hg^{2+} and biothiols in complex matrices. Chem. Commun. 48, 1147–1149.
Ziarati, A., Safaei-Ghomi, J., Rohani, S., 2013. Sonochemically synthesis of pyrazolones using reusable catalyst CuI nanoparticles that was prepared by sonication. Ultrason. Sonochem. 20, 1069–1075.